1-1-1999

Effects of laser mode and scanning direction on melt pool shape

K. Farooq
University of Central Florida

A. Kar
University of Central Florida

Effects of laser mode and scanning direction on melt pool shape

Cite as: Journal of Applied Physics **85**, 6415 (1999); https://doi.org/10.1063/1.370145
Submitted: 10 September 1998 . Accepted: 29 January 1999 . Published Online: 22 April 1999

K. Farooq, and A. Kar

Effects of laser mode and scanning direction on melt pool shape

K. Farooq and A. Kar
Center for Research & Education in Optics and Lasers (CREOL), Mechanical, Materials and Aerospace Engineering Department, University of Central Florida, 4000 Central Florida Boulevard, Orlando, Florida 32816-2700

(Received 10 September 1998; accepted for publication 29 January 1999)

A three-dimensional quasi-steady-state mathematical model is presented for laser heating with a multimode beam. The effects of laser beam scanning direction on the melt pool shape are investigated through the conduction analysis without phase change. The maximum temperature is found to be behind the center of the focal spot due to advection. The isotherms ahead of the focal spot bunch together and spread apart behind the focal spot on the surface of the workpiece due to the same effect. The temperature profile shows four distinct peaks as a result of four intensity peaks. Scanning direction affects the melt pool shape which needs to be considered for high precision cutting applications such as integrated circuit cutting. The melt pool shape is found to be symmetric about the x axis in the x-y plane and z axis in the y-z plane for the scanning angles $\phi_s = 0°$ and $-90°$, however it is asymmetric for other scanning angles. © *1999 American Institute of Physics.* [S0021-8979(99)05909-5]

I. INTRODUCTION

The polarization of laser and its mode structure affect the heat distribution during laser materials processing. For most lasers focal spot consists of several TEM_{mn} modes, and therefore, the energy distribution at the focal spot is nonuniform and localized hot spots are generated at the substrate surface. In this article, three dimensional heat conduction equation is solved for multimode laser beam. The effects of scanning direction on the melt pool shape are investigated. The latent heat of melting is taken into account by considering an effective specific heat capacity. The melt pool shape here refers to the shape of the melting temperature isotherm.

The laser beam profile is characterized by its transverse electromagnetic mode which is denoted by TEM_{mn}. m and n are the mode numbers in two perpendicular directions that are orthogonal to the direction of laser beam propagation. The values of m and n, that is, the mode structure, depend on the cavity design. For rectangular cavities, such as the chemical oxygen–iodine laser (COIL) resonator the amplitude of the standing wave pattern is given by the Hermite–Gaussian polynomial and for cylindrical cavities it is given by Laguere–Gaussian polynomial. The intensity distribution is related to the square of the amplitude. Generally, circular output apertures produce a laser beam of cylindrical symmetry whose mode structure is expressed in terms of cylindrically symmetric Laguerre–Gaussian modes. However, the presence of a Brewster window or of any other rectangular asymmetries in the mirror coatings or the laser gain medium or structural alignment of the laser cavity would generate rectangular beams whose mode structure is expressed in terms of rectangularly symmetric Hermite–Gaussian modes.[1] It is a common experimental observation that single higher order Hermite–Gaussian modes are more easily obtainable in stable laser resonators than are higher order Laguerre–Gaussian modes, even in resonators with apparently cylindrical symmetry. Both theoretical and experimental studies have confirmed that even very small deviations from cylindrical symmetry breaks the degeneracy of cylindrical Laguerre–Gaussian modes, transforming them into nondegenerate Hermite–Gaussian modes.[2,3] For this reason, the Hermite–Gaussian polynomial is used in this study to express the laser irradiance.

The mode number affects the focusability of a laser beam. The higher the number of modes, the more difficult it is to focus the beam since the beam no longer comes from a single spot. With proper design of the resonator higher order modes can be eliminated. In many applications such as laser surface hardening and cladding, higher order modes are desirable for uniform heating. TEM_{00} mode is best suited for laser cutting, drilling, and welding applications.[4]

The absorptivity of the material is affected by the polarization. If polarization is perpendicular to the scanning direction, a shallow but wider cut is obtained. The directional effects in laser cutting can be avoided by using circularly polarized light.[4] Wallace *et al.*[5] attributed the curvature of laser machined grooves in Si_2O_3 to the polarization of light.

The propagation of heat in the workpiece is encountered in all laser materials processing. Kar *et al.*[6] have studied the conduction heat distribution for materials processing with two multimode laser beams. Pecharapa and Kar[7] developed a simple model for weld depth and width and presented simple expressions for the solid–liquid and liquid–vapor interfaces. Nissim *et al.*[8] studied the effects of scanning circular and elliptical spots for processing semiconductor materials. For a Gaussian beam moving with constant velocity, the heat conduction equation is solved by Cline and Anthony[9] using Green's function for a medium that was semi-infinite in one direction and infinite in other two directions. For a Gaussian beam irradiating a cylindrical medium, the steady-state heat conduction equation was solved by Lax[10,11] by considering both constant and temperature dependent thermophysical properties. The case with temperature dependent thermo-

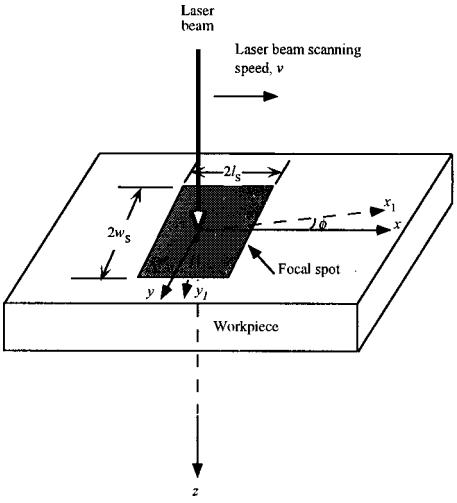

FIG. 1. The laser spot in relation to the rotated (x_1,y_1) and unrotated (x,y) coordinates, scanning in the positive x direction with a constant speed v. For further detail see Fig. 2.

physical properties was solved using Kirchhoff's transformation. Xie and Kar[12] studied large-area film removal with a multimode chemical oxygen–iodine laser. A transient thermal model was developed by Kar and Mazumder[13] to predict temperature distribution in finite slabs by considering temperature dependent thermophysical properties and a Gaussian laser beam. Oronzio *et al.*[14] presented an analytic solution to the three-dimensional quasistationary problem in a finite depth and width with a circular Gaussian moving heat source at the body surface. The densification of ceramic coating by a moving TEM_{00} mode laser was studied by Cheng and Kar[15] by analyzing three-dimensional quasi-steady-state heat conduction using Fourier integral transform. Moody and Handel[16] used a numerical algorithm to determine the temperature distribution in an infinite medium during laser heating. Xie and Kar[17] studied the one-dimensional heat conduction problem to analyze melting during laser materials processing. They solved the problem approximately to express melt depth as a function of various process parameters. Gratzke *et al.*[18] investigated the three-dimensional time-dependent temperature distribution in a moving solid of finite thickness due to a laser beam of Gaussian power distribution on its surface. The effects due to latent heat and key hole were neglected.

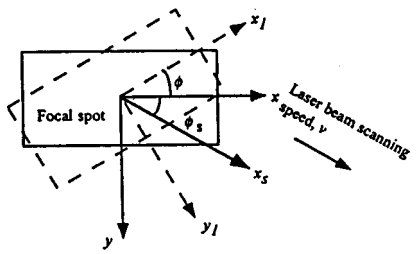

FIG. 2. The focal spot is rotated through an angle ϕ, and is scanned along the positive x direction with a constant speed v. It has the same heating effect as keeping the focal spot unrotated and scanning it at an angle ϕ_s, along x_s direction with a constant speed v, such that $\phi_s = -\phi$.

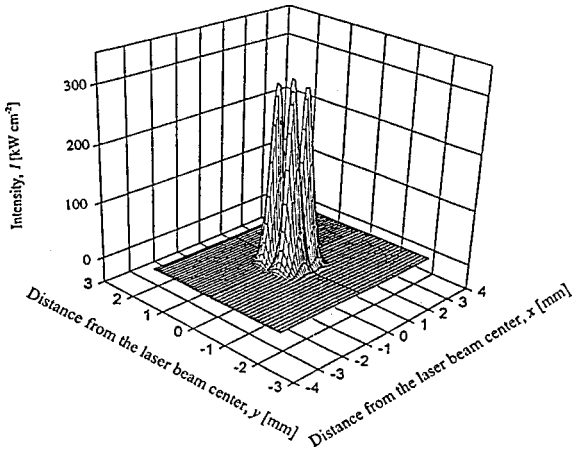

FIG. 3. Intensity distribution ($P=2$ kW) at the focal spot for a laser beam (TEM_{mn}, $m=0,1$, and $n=0,1$) of spot size $2l_s=1.7$ mm and $2w_s=1.2$ mm, moving in positive x direction with a speed $v=1$ m/min. Scanning angle $\phi_s=0$.

II. MATHEMATICAL MODEL

The heating of a workpiece with multimode laser beam is different from the heating with a TEM_{00} mode beam. This is because the multimode beam produces multiple localized hot spots, whereas the TEM_{00} mode beams generate a single central hot spot. Kar *et al.*[6] studied the effect of laser mode structure on heating. The present study investigates the effects of multimode laser beam scanning direction on heating. The heat conduction equation for a heat source moving with a velocity v in x direction relative to the workpiece, under the quasi-steady-state condition can be written as

$$\alpha_e\left(\frac{\partial^2 T}{\partial x^2}+\frac{\partial^2 T}{\partial y^2}+\frac{\partial^2 T}{\partial z^2}\right)=-v\,\frac{\partial T}{\partial x} \tag{1}$$

for $-\infty \leqslant x \leqslant \infty$, $-\infty \leqslant y \leqslant \infty$, and $0 \leqslant z \leqslant \infty$. It may be noted that in Eq. (1) an effective thermal diffusivity α_e is considered which is defined in terms of thermal conductivity k,

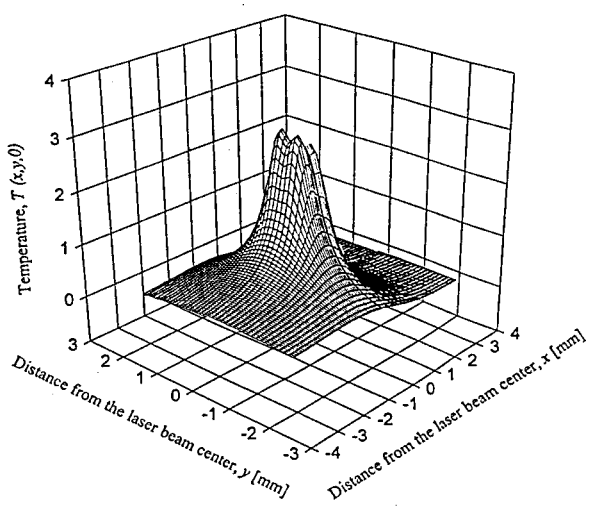

FIG. 4. Temperature distribution ($P=2$ kW, $A=0.45$) at the top of workpiece ($z=0$), for a laser beam (TEM_{mn}, $m=0,1$, and $n=0,1$) of spot size $2l_s=1.7$ mm and $2w_s=1.2$ mm, moving in positive x direction with a speed $v=1$ m/min. Scanning angle $\phi_s=0$.

density ρ, and effective specific heat c_{pe} as $\alpha_e = k/(\rho c_{\text{pe}})$. Since model does not take into account the melting effect, the latent heat of melting is incorporated into the effective specific heat to somewhat account for it. The effective specific heat c_{pe} in turn is defined in terms of specific heat c_p, latent heat of melting L_m, and the melting temperature T_m of the substrate as $c_{\text{pe}} = c_p + L_m/T_m$. Equation (1) is written in a moving coordinate system such that the center of the laser beam is coincident with the origin. The x, y, and z coordinates are defined such that the x-y plane lies on the top of the workpiece and the positive z axis is into the workpiece as shown in Fig. 1. Another set of axes x_1 and y_1 are so chosen that its origin lies at the beam center and the x_1 and y_1 axes are parallel to the length and width of the rectangular spot, respectively. The laser beam is scanned along the x axis at a constant velocity v. When the beam is rotated by an angle ϕ from the x axis, the x_1 and y_1 axes are also rotated so that they subtend an angle ϕ with the x and y axes, respectively. This situation is equivalent to keeping the length and width of laser spot parallel to the x and y axes, respectively, and scanning the beam in the x_s direction at scanning angle $\phi_s = -\phi$ (see Fig. 2). The relationship between the rotated coordinate system (x_1, y_1) and the original coordinate system (x,y) is given by:[19]

$$x_1 = x\cos\phi + y\sin\phi, \tag{2a}$$

$$y_1 = y\cos\phi - x\sin\phi. \tag{2b}$$

The temperature $T(x,y,z)$ is a normalized temperature defined by

$$T = \frac{T_1 - T_0}{T_m - T_0}, \tag{3}$$

where T_1 and T_0 are the substrate and ambient temperatures, respectively.

The boundary conditions for the above differential equation are

$$T \to 0 \quad \text{as} \quad x \to \pm\infty \tag{4a}$$

$$T \to 0 \quad \text{as} \quad y \to \pm\infty \tag{4b}$$

$$T \to 0 \quad \text{as} \quad z \to \infty \tag{4c}$$

$$k\frac{\partial T}{\partial z} = -\frac{1}{T_m - T_0} I, \quad \text{at} \quad z = 0. \tag{4d}$$

The laser irradiance I is given by $I = \Sigma_{m=0}^{M}\Sigma_{n=0}^{N} I_{mn}$, M and N are the largest mode numbers in the x_1 and y_1 directions, respectively. I_{mn} is the irradiance of the laser beam of mth and nth order:

$$I_{mn} = \frac{2AP_{mn}}{\pi 2^{m+n} m!\,n!\,l_0 w_0} H_m^2\left(\frac{\sqrt{2}x_1}{l_0}\right) H_n^2\left(\frac{\sqrt{2}y_1}{w_0}\right) \times \exp\left(-\frac{2x_1^2}{l_0^2}\right)\exp\left(-\frac{2y_1^2}{w_0^2}\right). \tag{5}$$

P_{mn} is the total power of the laser of mth and nth order modes. l_0 and w_0, are, respectively, the half length and half width of the Gaussian mode of the beam. They are given by $l_0 = l_s/\sqrt{2m+1}$ and $w_0 = w_s/\sqrt{2n+1}$ where l_s and w_s are, respectively, the half length and half width of the rectangular laser spot. A is the absorptivity of the material. H_m and H_n are the mth and nth degree Hermite polynomials.

TABLE I. Typical values of thermophysical properties of iron. Due to the lack of availability of high temperature data, these values were used in this study to obtain various results for 400 series stainless steel workpiece (Ref. 20).

Thermophysical properties	Values of thermophysical properties
Melting point, T_m	1809 K
Specific heat, c_p	456 J $\text{Kg}^{-1}\,\text{K}^{-1}$
Thermal conductivity, k	78.2 W $\text{m}^{-1}\,\text{K}^{-1}$
Thermal diffusivity, $\alpha = k/(\rho c_p)$	2.18×10^{-5} $\text{m}^2\,\text{s}^{-1}$
Effective thermal diffusivity, $\alpha_e = k/(\rho c_{\text{pe}})$	1.64×10^{-5} $\text{m}^2\,\text{s}^{-1}$
Latent heat of melting, L_m	2.72×10^{5} J/Kg^{-1}

Using the definition of I and substituting Eqs. (2a) and (2b) into Eq. (5), the following expression is obtained:

$$I = \sum_{m=0}^{M}\sum_{n=0}^{N} \frac{2AP_{mn}}{\pi 2^{m+1} m!\,n!\,l_0 w_0} H_m^2\left(\frac{\sqrt{2}(x\cos\phi + y\sin\phi)}{l_0}\right) \times H_n^2\left(\frac{\sqrt{2}(y\cos\phi - x\sin\phi)}{w_0}\right) \times \exp\left(\frac{-2(x\cos\phi + y\sin\phi)^2}{l_0^2}\right) \times \exp\left(\frac{-2(y\cos\phi - x\sin\phi)^2}{w_0^2}\right). \tag{6}$$

By using the heat flux I in from Eq. (6) in the three-dimensional heat conduction model of Kar *et al.*,[6] the temperature distribution in the substrate is shown to be

$$T(x,y,z) = \frac{1}{2\pi}\int_{-\infty}^{\infty}\int_{0}^{2\pi} f(x - r'\cos\theta, y - r'\sin\theta) \times \exp(-br'\cos\theta)\frac{\exp(-b\sqrt{r'^2+z^2})}{\sqrt{r'^2+z^2}} r'\,dr'\,d\theta, \tag{7}$$

where $r' = \sqrt{x'^2 + y'^2}$, $f(x - r'\cos\theta, y - r'\sin\theta)$ written in the polar form, follows from $f(x,y)$ given by

TABLE II. Power distribution in various modes (kW).

	n	
m	0	1
0	0.1	0.5
1	0.15	1.25

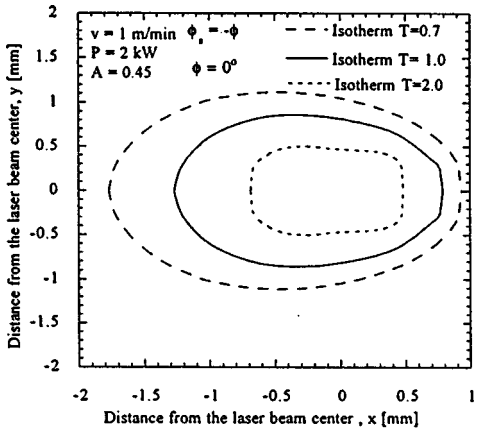

FIG. 5. Top surface ($z=0$) isotherms for a laser beam (TEM_{mn}, $m=0,1$, and $n=0,1$) of spot size $2l_s=1.7$ mm and $2w_s=1.2$ mm, moving in positive x direction with a speed v and scanning angle $\phi_s=0$.

$$f(x,y)=\sum_{m=0}^{M}\sum_{n=0}^{N}\frac{2AP_{mn}}{k(T_m-T_0)\pi 2^{m+1}m!n!l_0w_0}\times H_m^2\left(\frac{\sqrt{2}(x\cos\phi+y\sin\phi)}{l_0}\right)\times H_n^2\left(\frac{\sqrt{2}(y\cos\phi-x\sin\phi)}{w_0}\right)\times\exp\left(\frac{-2(x\cos\phi+y\sin\phi)^2}{l_0^2}\right)\times\exp\left(\frac{-2(y\cos\phi-x\sin\phi)^2}{w_0^2}\right) \tag{8}$$

and

$$b=\frac{v}{2\alpha_e}. \tag{9}$$

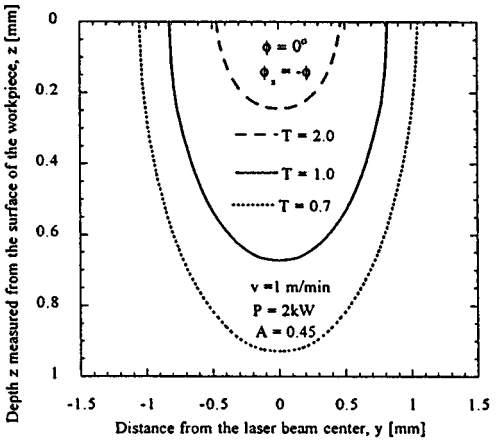

FIG. 6. Isotherms in the y-z plane at $x=0$, for a laser beam (TEM_{mn}, $m=0,1$, and $n=0,1$) of spot size $2l_s=1.7$ mm and $2w_s=1.2$ mm. Scanning angle $\phi_s=0$.

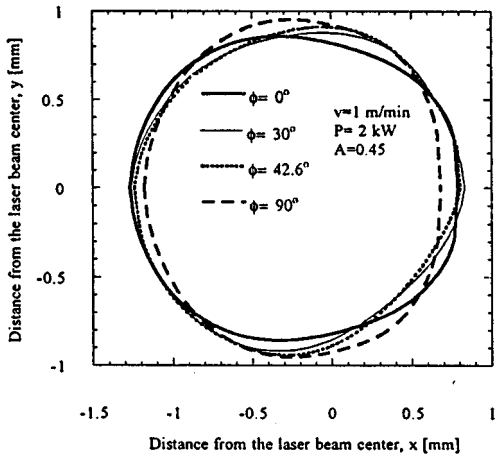

FIG. 7. Melt pool shapes ($z=0$) for the laser beam (TEM_{mn}, $m=0,1$, and $n=0,1$) of spot size $2l_s=1.7$ mm and $2w_s=1.2$ mm for different scanning angles, $\phi_s=-\phi$.

Equation (7) is used to numerically evaluate the temperature distribution $T(x,y,z)$ by using the trapezoidal rule for numerical integration.

III. RESULTS AND DISCUSSION

The above mathematical model is valid for any multimode spot but in this study only TEM_{mn}, $m=0,1$, and $n=0,1$ modes are considered. The total power P, absorptivity A, and scanning velocity v in this study are 2 kW, 0.45 and 1 m/min, respectively. The dimensions of the rectangular spot are, $2l_s=1.7$ mm and $2w_s=1.2$ mm. The thermophysical properties of the substrate and the distribution of power in various laser modes are given in Tables I and II, respectively. These data are used to determine the temperature distribution from Eq. (7). Figure 3 shows the intensity distribution in the multimode beam when scanning angle $\phi_s=0°$, that is the laser beam is scanned along the x axis. Four peaks in this figure indicate that the laser energy distribution is nonuniform. The peak intensities occurs at the points $x=\pm 0.3091$ mm and $y=\pm 0.2842$ mm. Figure 4 is the dimen-

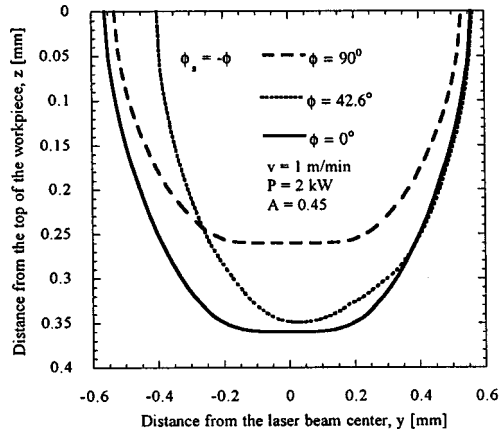

FIG. 8. Melt pool shapes at the slice $x=0.6$ mm for the laser beam (TEM_{mn}, $m=0,1$, and $n=0,1$) of spot size $2l_s=1.7$ mm and $2w_s=1.2$ mm for different scanning angles, $\phi_s=-\phi$.

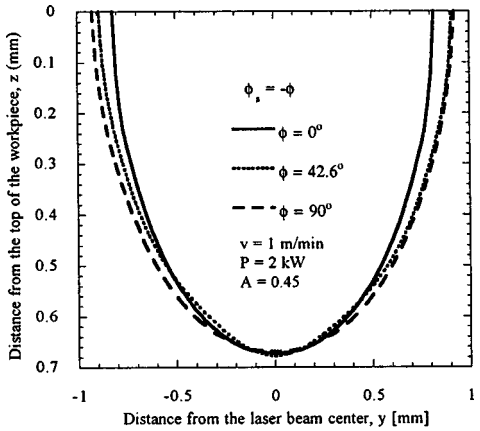

FIG. 9. Melt pool shapes at the slice $x=0$ mm for the laser beam (TEM_{mn}, $m=0,1$, and $n=0,1$) of spot size $2l_s=1.7$ mm and $2w_s=1.2$ mm for different scanning angles, $\phi_s=-\phi$.

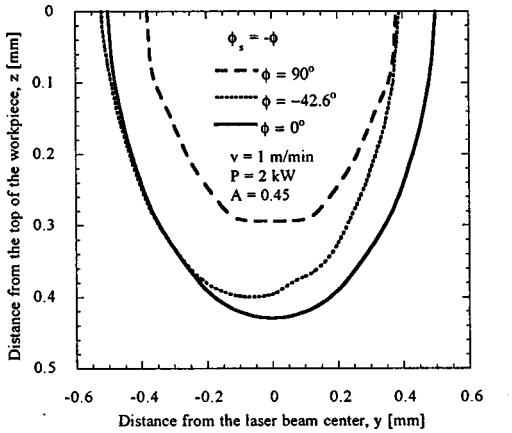

FIG. 11. Melt pool shapes at the slice $x=-1.1$ mm for the laser beam (TEM_{mn}, $m=0,1$, and $n=0,1$) of spot size $2l_s=1.7$ mm and $2w_s=1.2$ mm for different scanning angles, $\phi_s=-\phi$.

sionless temperature distribution corresponding to this intensity distribution. The maximum temperature occurs behind the laser beam center because of advection due to the relative motion between the beam and workpiece.

Figure 5 shows various isotherms ($T=0.7$, 1.0, 2.0) at the top surface ($z=0$) when the laser is scanned in the positive x direction (scanning angle $\phi_s=0°$). The isotherms are symmetric about the x axis. They cluster in front of the laser beam and spread apart behind the beam. The isotherm $T=1$ corresponds to the melting temperature, and the inner isotherm $T=2.0$ is almost rectangular corresponding to the shape of the temperature mound shown in Fig. 4. Figure 6 shows the isotherms in the z direction for a slice in the y-z plane at $x=0$. The isotherms are symmetric about the z axis in the transverse plane as the laser focal spot is symmetric about the x axis for scanning angle $\phi_s=0$. Figure 7 shows the melt pool boundary at the substrate surface ($z=0$) for scanning angle $\phi_s=0°$, $-30°$, $-42.6°$, and $-90°$. The length and width of the laser spot are aligned to the x direction for $\phi_s=0°$ and $-90°$, respectively. The melt pool is symmetric about the x axis for $\phi_s=0°$ and $-90°$, and it is asymmetric for $\phi_s=-30°$ and $-42.6°$. The significance of $\phi_s=-42.6°$ is that the diagonal elements of the focal spot of this study are aligned to the scanning direction at this angle. The width of the melt pool for $\phi_s=-42.6°$ is bigger than for $\phi_s=-30°$ but smaller than for $\phi_s=-90°$.

Figures 8–11 show the transverse sections of the melt pool for the slices taken at $x=0.6$, 0, -0.345, and -1.1 mm for $\phi_s=0°$, $-42.6°$, and $-90°$. They demonstrate the variations in the melt pool depth and width for various scanning angles. The deepest melt pool is obtained for $x=-0.345$ mm when $\phi_s=0°$. The differences in the melt widths as well as depths are relatively large ahead of and behind the laser beam center. Figures 12 and 13 compare the proposed model with the Rosenthal[21] model. The figures show that the results of both models are qualitatively similar. The numerical values are different because the Rosenthal model is based on the assumption that the laser beam is a point heat source, and therefore, it under estimates the melt width and over estimates the melt depth. The percentage increase in the maximum melt pool width relative to $\phi=0°$ indicates that changing the beam orientation angle ϕ to 30°, 42.6°, and 90° leads to 2.2%, 5.4%, and 8.7% increase in the maximum melt pool width (kerf width) respectively. Since

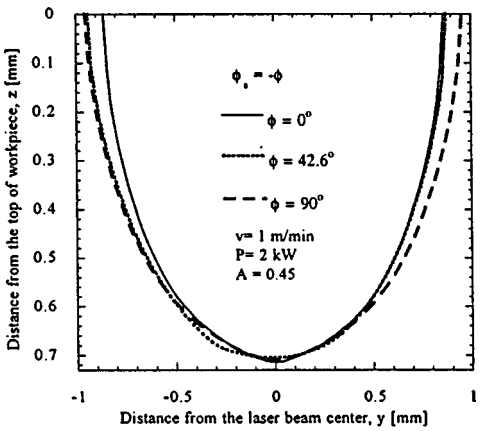

FIG. 10. Melt pool shapes at the slice $x=-0.345$ mm for the laser beam (TEM_{mn}, $m=0,1$, and $n=0,1$) of spot size $2l_s=1.7$ mm and $2w_s=1.2$ mm for different scanning angles, $\phi_s=-\phi$.

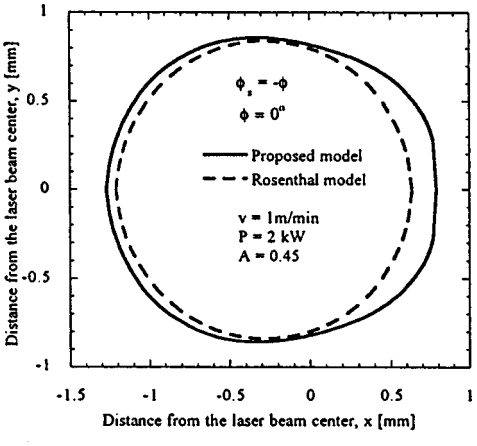

FIG. 12. Melt pool comparison ($z=0$) between proposed model and Rosenthal model. The laser beam (TEM_{mn}, $m=0,1$, and $n=0,1$) of spot size $2l_s=1.7$ mm and $2w_s=1.2$ mm is used for proposed model.

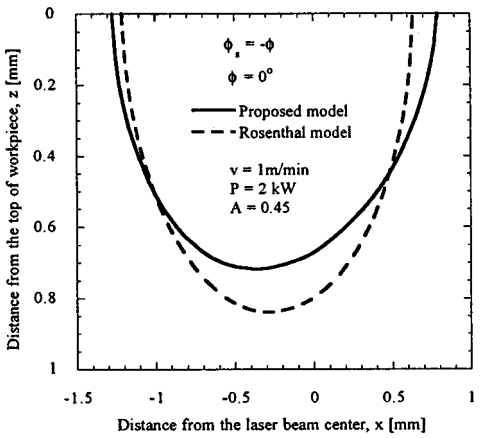

FIG. 13. Melt pool comparison ($y=0$) between proposed model and Rosenthal model. The laser beam (TEM_{mn}, $m=0,1$, and $n=0,1$) of spot size $2l_s=1.7$ mm and $2w_s=1.2$ mm is used for proposed model.

$\phi_s=-\phi$, the laser beam scanning direction should be taken into account while cutting delicate parts such as integrated circuits.

IV. CONCLUSIONS

The laser-mode based model can be applied to any TEM_{mn} beam however model results are investigated for $m=0,1$ and $n=0,1$. The maximum temperature is found to be behind the center of the focal spot due to advection. The isotherms ahead of the focal spot bunch together and spread apart behind the focal spot on the surface of the workpiece due to the same effect. The temperature profile shows four distinct peaks as a result of four intensity peaks.

The scanning direction affects the melt pool shape. It is critical in precision cutting application such as cutting integrated circuits. The melt pool shapes for four different scanning angles $\phi_s=0°$, $-30°$, $-42.6°$, and $-90°$ are investigated. The maximum depth and width of the melt pool is found to be behind the focal spot center due to advection. At $\phi_s=0°$ the length of the focal spot $2l_s=1.7$ mm is along the x axis and its width $2w_s=1.2$ mm is along the y axis where as the origin lies at the center of the focal spot. The melt pool shape is found to be symmetric about the x axis in the x-y plane and z axis in the y-z plane for the scanning angles $\phi_s=0°$ and $-90°$, however it is asymmetric for other scanning angles.

At scanning angle $\phi_s=-90°$, the melt pool is found to be widest and shallowest and the opposite is true for $\phi_s=0°$. An increase of 8.7% in the maximum melt pool width was observed for $\phi_s=-90°$ relative to $\phi_s=0°$ for $P=2$ kW, $v=1$ m/min, and $A=0.45$. The significance of $\phi_s=-42.6°$ is that diagonal intensity peaks on the focal spot get aligned in the scanning direction. At this angle the melt pool is widest for any scanning angle between 0° and 90°. The differences in the melt pool shapes in the x-y plane ($z=0$) and y-z plane for different scanning angles ϕ_s are more apparent as we move farther from the origin on the x axis.

The comparison of the melt pool shape of the proposed model with the Rosenthal model indicates that the melt pool shape is qualitatively same as that of Rosenthal model and validates the theory.

[1] A. E. Siegman and S. W. Townsend, IEEE J. Quantum Electron. **29**, 1212 (1993).
[2] J. P. Goldsborough, Appl. Opt. **3**, 267 (1964).
[3] C. Fabre, R. G. DeVoe, and R. G. Brewer, Opt. Lett. **11**, 365 (1986).
[4] G. Chryssolouris, *Laser Machining Theory and Practice* (Springer, New York, 1991), pp. 42–43, 48, 58–59.
[5] R. J. Wallace, M. Bass, and S. M. Copley, J. Appl. Phys. **59**, 3555 (1986).
[6] A. Kar, J. E. Scott, and W. P. Latham, J. Appl. Phys. **80**, 667 (1996).
[7] W. Pecharapa, and A. Kar, J. Phys. D **30**, 3322 (1997).
[8] Y. I. Nissim, A. Lietoila, and R. B. Gold, J. Appl. Phys. **51**, 274 (1980).
[9] H. E. Cline and T. R. Anthony, J. Appl. Phys. **48**, 3895 (1977).
[10] M. Lax, J. Appl. Phys. **48**, 3919 (1977).
[11] M. Lax, Appl. Phys. Lett. **33**, 786 (1978).
[12] J. Xie and A. Kar, J. Appl. Phys. **82**, 4744 (1997).
[13] A. Kar and J. Mazumder, J. Appl. Phys. **65**, 2923 (1989).
[14] M. Oronzio, M. Biagio, and N. Vincenzo, Int. J. Heat Mass Transf. **38**, 1305 (1995).
[15] J. Cheng and A. Kar, J. Mater. Sci. **32**, 6269 (1997).
[16] J. E. Moody and R. H. Hendel, J. Appl. Phys. **53**, 4364 (1982).
[17] J. Xie and A. Kar, J. Appl. Phys. **81**, 3015 (1997).
[18] U. Gratzke, P. D. Kapadia, and J. Dowden, J. Phys. D **24**, 2125 (1991).
[19] M. R. Spiegel, *Mathematical Handbook*, Schaum's outline series (McGraw–Hill, New York, 1992), p. 36.
[20] E. A. Brandes, *Smithells Metal Reference Book* (Butterworth, Boston, 1983), pp. 8–2 and 14–1.
[21] D. Rosenthal, Weld. J. **20**, 220s (1941).